ASTRO-PH/0010489
Preprint typeset using LaTeX style emulateapj v. 21/08/00

ON THE MASS AND INCLINATION OF THE PSR J2019+2425 BINARY SYSTEM

David J. Nice and Eric M. Splaver
Physics Department, Princeton University
Box 708, Princeton, NJ 08544
dnice@princeton,edu, esplaver@princeton.edu

AND

Ingrid H. Stairs[1]
Jodrell Bank Observatory, University of Manchester
Jodrell Bank, Macclesfield, Cheshire, SK11 9DL, United Kingdom
istairs@gb.nrao.edu

Accepted by the Astrophysiccal Journal, 24 October 2000

ABSTRACT

We report on nine years of timing observations of PSR J2019+2425, a millisecond pulsar in a wide 76.5 day orbit with a white dwarf. We measure a significant change over time of the projected semi-major axis of the orbit, $\dot{x}/x = 1.3 \pm 0.2 \times 10^{-15}\,\mathrm{s}^{-1}$, where $x \equiv (a_1 \sin i)/c$. We attribute this to the proper motion of the binary. This constrains the inclination angle to $i < 72°$, with a median likelihood value of 63°. A similar limit on inclination angle arises from the lack of a detectable Shapiro delay signal. These limits on inclination angle, combined with a model of the evolution of the system, imply that the neutron star mass is at most $1.51\,M_\odot$; the median likelihood value is $1.33\,M_\odot$. In addition to these timing results, we present a polarization profile of this source. Fits of the linear polarization position angle to the rotating vector model indicate the magnetic axis is close to alignment with the rotation axis, $\alpha < 30°$.

Subject headings: stars: neutron—binaries: general—pulsars: individual (PSR J2019+2425)

1. INTRODUCTION

Neutron star masses measured in radio pulsar binary systems are consistent with a remarkably small range, $m = 1.35 \pm 0.04\,\mathrm{M}_\odot$ (Thorsett & Chakrabarty 1999). The best such measurements, those with uncertainty less than 5%, are of pulsars in tightly bound, highly eccentric neutron star–neutron star binaries. In such systems, relativistic phenomena detected in radio pulse timing experiments allow the direct, high precision measurement of the masses of the component stars. By contrast, measurement of masses of pulsars in neutron star–white dwarf systems tend to have lower precision, or to be statistical in nature. Measurement of masses in these systems are of interest because their evolution is substantially different from that of neutron star–neutron star binaries. In particular, neutron star–white dwarf systems go through an extended period of mass transfer, during which the secondary loses several tenths of a solar mass of matter, at least some of which is accreted onto the neutron star, making the system visible as a low mass X-ray binary. Thus, one might expect the neutron stars in these systems to be more massive than those in neutron star–neutron star binaries.

In this paper, we describe pulse timing observations of PSR J2019+2425, a millisecond pulsar in a 76.5 day orbit with a white dwarf. Our observations constrain the (*a priori* unknown) inclination angle of the orbit. By combining this constraint with a theory of orbital evolution, we determine an upper limit of the mass of the pulsar.

We have previously reported on this pulsar in Nice & Taylor (1995). The present work represents a tripling of the time span of the observations. In §2 we describe the data acquisition. In §3 we present an analysis of the pulse arrival times. Implications for the neutron star mass are given in §4. Polarimetry of the pulsar is discussed in §5.

2. OBSERVATIONS

2.1. *Data collection*

We measured times of arrival (TOAs) of pulses from PSR J2019+2425 on 78 separate days between 1 October 1991 and 7 August 2000, using the 305 m radio telescope at Arecibo. We made all observations at 430 MHz, primarily with the telescope's line feed, except for a few of the most recent observations, for which we used the Gregorian 430 MHz receiver.

We employed two distinct data acquisition systems. Between October 1991 and November 1994, we used the Princeton Mark III data acquisition system (Stinebring *et al.* 1992). An analog filter bank divided an 8 MHz passband into thirty-two 0.25 MHz spectral channels in each sense of circular polarization. These signals were detected with 100 μs time constants, and opposite polarizations were summed. The resulting intensity levels were sampled and summed synchronously with the pulsar period. Pulse profiles were accumulated for integration times of 2–3 minutes and stored for later analysis. Off-line, profiles from different spectral channels were shifted in time to compensate for interstellar dispersion and summed to produce a single de-dispersed profile for each integration. A combination of differential dispersion smearing within the spectral channels and analog filter bank time constants limited the time resolution of these profiles to 450μs.

---

[1] Present address: NRAO, Box 2, Green Bank, WV 24944

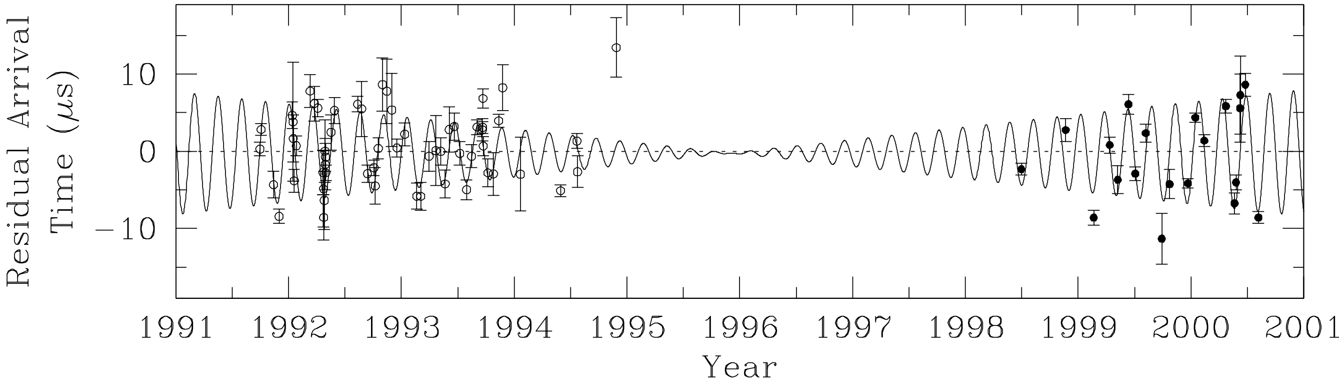

FIG. 1.— Residual pulse arrival times after removing the timing model in table 1 but with constant projected semi-major axis ($\dot{x} \equiv 0$). Open and closed circles indicate Mark III and Mark IV data, respectively. The solid line shows the residual arrival times expected from the changing apparent orbital size, $\dot{x} = 5 \times 10^{-14}$; this curve is sinusoidal with the orbital period with amplitude increasing linearly towards the ends of the data set. Arrival time uncertainties shown in the figure do not include corrections for systematics.

No observations were made between November 1994 and June 1998 due to the Arecibo telescope upgrade project.

Between July 1998 and August 2000, observations were made as part of the Arecibo coordinated timing project. We used the Princeton Mark IV system for data collection (Stairs *et al.* 2000). In each sense of circular polarization, a 5 MHz passband was mixed to baseband using local oscillators in phase quadrature. The four resulting signals were low-pass filtered at 2.35 MHz, sampled at 5 MHz, quantized to 4 bits, and stored on disk or tape. Upon playback, these voltages were coherently dedispersed using software techniques. Self- and cross-products of the complex voltages were calculated, giving power measurements in four Stokes parameters. These were summed synchronously with the pulse period with integration times of 190 seconds, yielding pulse profiles with full polarimetry. The profiles were calibrated by measurement of a pulsed noise calibration signal injected at the telescope receiver at the start or end of each observation; the noise calibration signals themselves were calibrated against continuum radio sources.

2.2. *Time of arrival measurements*

We derived TOAs by fitting a standard template to the total intensity de-dispersed profiles. Separate standard templates were used for the Mark III and Mark IV data sets. The locations of the pulse peak measured in the fit were added to the scan start times to produce TOAs. For pre-upgrade observations, the start times were referenced to an observatory clock, which we corrected to UTC(NIST) and, ultimately, UTC. For post-upgrade observations, start times were referenced to GPS time, which tracks UTC within tens of nanoseconds, sufficient precision for our purposes.

We fit for an arbitrary offset between the Mark III and Mark IV TOAs. The measured offset, $43 \pm 3\,\mu$s, results from a combination of differences in signal propagation time through the hardware and differences in the standard templates used for measuring TOAs.

The set of TOAs from each day of observations were combined into a single effective TOA for that day. Days with very high uncertainties or few measurements were eliminated. The final data set consisted of 78 TOAs, of which 58 were taken with Mark III (1991–1994) and 20 were taken with Mark IV (1998–2000).

2.3. *TOA uncertainties*

An uncertainty was calculated for each daily TOA based on the scatter of the arrival times within that day. The root-mean-square of the uncertainties thus calculated was $1.4\,\mu$s for both the Mark III and Mark IV data. (While the time resolution of the Mark IV data was much higher than that of the Mark III data, the Mark III observations had a larger bandwidth and, usually, a substantially longer on-source time, resulting in similar overall precision.) In the timing analysis described below, we found the χ^2 values to be systematically high, $\chi^2/\nu = 3.3$, where ν is the number of degrees of freedom of the fit. There was no evidence of long-term or orbit-dependent trends in the pulse arrival times, suggesting the high χ^2 values are day-to-day jitter in our measurements, or systematic underestimates of our uncertainties, of unknown origin. We compensated for this by adding $2.4\,\mu$s in quadrature to the statistical uncertainty calculated on each day, which yielded fits with $\chi^2/\nu \approx 1$. By varying this systematic term independently for the Mark III and Mark IV data while analyzing separate χ^2 statistics for these two subsets of the data, we found that similar quadrature terms were needed for both subsets.

3. TIMING ANALYSIS

3.1. *Timing model and* $\dot{x}$

We used the TEMPO[2] software package to fit a pulse timing model to the observed TOAs. A standard

---

[2] http://pulsar.princeton.edu/tempo

TABLE 1

PARAMETERS OF PSR J2019+2425 SYSTEM[a]

Right ascension, α (J2000)	$20^{\mathrm{h}}19^{\mathrm{m}}31^{\mathrm{s}}.94900(3)$
Declination, δ (J2000)	$+24^\circ 25' 15''.3038(5)$
Proper motion in R. A., $\mu_{\alpha *} = (d\alpha/dt)\cos\delta$ (mas/yr)	$-9.41(12)$
Proper motion in Dec., $\mu_\delta = d\delta/dt$ (mas/yr)	$-20.60(15)$
Period (ms)	3.93452408033124(11)
Period derivative (10^{-21})	7.0237(12)
Epoch (MJD)	50000.0000
Orbital period, P_b (days)	76.51163479(2)
Change rate of orbital period, $\dot{P}_b$	$-3(6) \times 10^{-11}$
Projected semi-major axis, x (lt-s)	38.7676297(8)
Change rate of projected semi-major axis, $\dot{x}$	$5.1(8) \times 10^{-14}$
Eccentricity	0.00011109(4)
Longitude of periastron, ω	$159^\circ.03(2)$
Time of periastron passage[b](MJD)	50054.6439021 ± 0.004
Dispersion measure[c](pc cm^{-3})	17.203
Mass function, f_1 ($M_\odot$)	0.0106865005(6)

[a] Values in parentheses are "2σ" uncertainties (95% confidence) in the last digit quoted.

[b] Highly covariant with longitude of periastron; value corresponds to $\omega = 159^\circ.0300000$.

[c] Held fixed at the value found by Nice, Fruchter, & Taylor (1993).

timing model incorporating spin-down (period and period derivative), astrometric parameters (position and proper motion), and five Keplerian parameters of the pulsar orbit (orbital period, semi-major axis projected into the line of sight, eccentricity, angle of periastron, and time of periastron passage) is not adequate to fully describe the observed TOAs. It is necessary to also allow a secular change in the projected semi-major axis, $\dot{x} = dx/dt$, where $x \equiv (a_1 \sin i)/c$, and a_1 is the semi-major axis of the pulsar orbit, i is the inclination of the angular momentum vector of the orbit relative to the earth–pulsar line-of-sight, c is the speed of light, and the dot indicates a time derivative. The need for a nonzero $\dot{x}$ is illustrated in figure 1. The measured value of $\dot{x}$ is

$$\dot{x} = (5.1 \pm 0.8) \times 10^{-14}. \qquad (1)$$

The full set of parameter values from the best timing model fit is listed in table 1. Uncertainties were calculated by a bootstrap procedure. Values given in the table are twice the formal uncertainties. Since all observations were made at a single radio frequency, the dispersion measure was held fixed in the timing analysis.

3.2. *Interpretation of* $\dot{x}$

The nonzero $\dot{x} = (1/c)\, d(a_1 \sin i)/dt$ could, in principle, result from a change in orbital size, a_1, or inclination angle, i, or a combination. First we will consider (and reject) the possibility of a change in a_1. Then we will analyze the implications of a change in inclination angle.

Peters (1964) calculates the change in orbital size of a system of two point masses under general relativity,

$$\dot{a}_1 = -\frac{64}{5} T_\odot^3 \frac{m_1 m_2^5}{(m_1+m_2)^3} \frac{1}{a_1^3} \frac{1}{(1-e^2)^{7/2}} \times \times \left(1 + \frac{73}{24}e^2 + \frac{37}{96}e^4\right), \qquad (2)$$

where $T_\odot = GM_\odot/c^3 = 4.925 \times 10^{-6}\,$s, m_1 and m_2 are the pulsar and white dwarf masses expressed in solar masses, e is the eccentricity, and a_1 is expressed in light-seconds. While m_1, m_2, and a_1 are not unambiguously known, we can estimate the magnitude of $\dot{a}_1$ by using $m_1 \sim 1.4\,\mathrm{M}_\odot$, $m_2 \sim 0.35\,\mathrm{M}_\odot$, and $a_1 \sim 40\,$lt-sec, from which $\dot{a}_1 \sim 3 \times 10^{-23}$. This is many orders of magnitude below the observed $\dot{x} = 5 \times 10^{-14}$.

More generally, for typical astrophysical processes within a binary system, $|\dot{a}_1/a_1|$ will be the same order of magnitude as $|\dot{P}_b/P_b|$, where P_b is the orbital period. Interpreting the observed value of $\dot{P}_b$ (table 1) as an upper limit, $|\dot{P}_b| < 9 \times 10^{-11}$, we have $|\dot{P}_b/P_b| < 1.4 \times 10^{-17}$. This is two orders of magnitude smaller than the observed $|\dot{x}/x| = 1.3 \times 10^{-15}$, so we conclude that the observed nonzero $\dot{x}$ is not caused by orbital evolution.

The nonzero $\dot{x}$ must arise because of a change in the observed inclination of the orbit. Kopeikin (1996) discusses how apparent changes in orbital parameters arise due to the relative motion of the binary and the observer. The situation is sketched in figure 2. A component of the proper motion lies in the plane formed by the line-of-sight

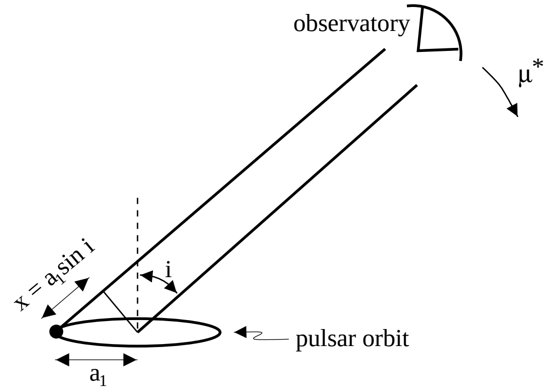

FIG. 2.— Geometry relevant to the observation of $\dot{x}$. See section § 3.2.

to the binary and the angular momentum vector of the binary. We write this as $\mu^* = \mu \sin\theta$, where μ is the total proper motion and $\theta = \theta_\mu - \Omega$ is the difference between the position angle of proper motion, θ_μ, and the position angle of the ascending node, Ω. It is clear that this component of proper motion equals the change in inclination angle, $\mu^* = di/dt$ (figure 2). From the definition of x,

$$\frac{\dot{x}}{x} = \mu \cot i \sin\theta. \tag{3}$$

The orientation of the binary, θ, is not known. However, requiring $|\sin\theta| < 1$ in equation 3 gives a firm upper limit on i. Using $\mu = 22.62 \pm 0.15\,\mathrm{mas/yr}$, $x = 38.7676\,\mathrm{lt\text{-}s}$, and $\dot{x} = 4.3 \times 10^{-14}$ (the lower limit of allowed values from table 1) in equation 3 yields

$$i < \tan^{-1}\left(\mu \frac{x}{\dot{x}}\right) = 72^\circ. \tag{4}$$

The distribution of inclination angles within this constraint can be studied using Monte Carlo analysis. We make the *a priori* assumption that all orientations of the binary system in space are equally likely. Under this assumption, θ is a uniformly distributed random variable and i is a random variable distributed with uniform probability in $\cos i$. We select values of θ and i from these distributions and retain only those combinations which satisfy equation 3 within the measurement uncertainties. In the resulting data set, the distribution of i is somewhat peaked towards the highest allowed values. The median likelihood inclination angle within this distribution is 63°. We discuss the implications of this in §4.

3.3. *Shapiro delay*

According to general relativity, the pulse signal is delayed as it propagates through the gravitational potential well of the secondary. This "Shapiro delay" for a pulsar in a circular orbit is

$$\Delta t = -2T_\odot m_2 \ln[1 - \sin i \sin\phi_b], \tag{5}$$

where ϕ_b is the orbital phase measured from the ascending node. For small inclination angles, the variation of Δt over the orbit is nearly sinusoidal, so it is indistinguishable from a slight increase in the (*a priori* unknown) orbital size, a_1. For edge-on orbits ($i \approx 90^\circ$), the variation in Δt becomes strongly peaked at $\phi_b \approx 90^\circ$, when the pulsar is behind the secondary; this breaks the covariance with the Keplerian orbital model and allows measurement of the Shapiro delay (and hence measurement of m_2 and i).

We did not detect the Shapiro delay in the PSR J2019+2425 TOAs. We can use this non-detection to place limits on allowed inclination angles. We analyzed the TOAs of PSR J2019+2425 using a grid of timing models, each of which incorporated the Shapiro delay signal appropriate for some inclination angle $0^\circ < i < 90^\circ$ and secondary mass $0 < m_2 < 0.8\,\mathrm{M}_\odot$. The fits to most such models yielded χ^2 values similar to a model with no Shapiro delay. However, models with high inclination angles and/or high secondary masses fared poorly—meaning that the Shapiro delay would have been detected had these been the true values of i and m_2. Figure 3 shows the parameter space excluded by models with $\Delta\chi^2 > 4$ (i.e., 2σ) relative to the base model. For modest secondary masses, the inclination angle limit is $i \lesssim 73^\circ$, very similar to the limit from the $\dot{x}$ measurement.

4. MASS

The observational limits on the inclination angle, combined with binary evolution theory, constrain the mass of the pulsar. Like all wide neutron star–white dwarf binaries, the PSR J2019+2425 system underwent an extended period of mass transfer, during which the pulsar was spun up to its short period. A straightforward model of this mass transfer gives a unique relation between the orbital period, P_b, and secondary mass, m_2 at the end of this phase of evolution (see Rappaport *et al.* 1995 and references therein.). Key elements of this model include (i) stable mass transfer, with the secondary filling its Roche lobe in the giant phase; (ii) well-defined dependence of the radius of the giant secondary on its core mass; and (iii) dissipation of almost all of the outer envelope of the secondary, so that the present day secondary mass, m_2, is only slightly more than the secondary core mass.

In a numerical analysis of systems which evolve into neutron star–white dwarf binaries, Tauris and Savonije (1999) found the relation between orbital period (in days) and secondary mass (in solar masses) to be

$$m_2 = \left(\frac{P_b}{b}\right)^{1/a} + c, \tag{6}$$

where a, b, and c depend on the chemical composition of

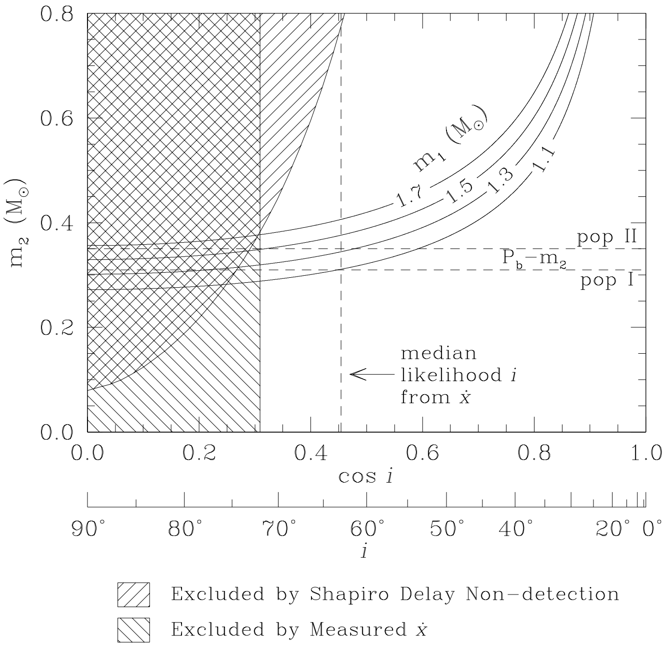

FIG. 3.— Constraints on the inclination angle, i, and white dwarf mass, m_2, from measured $\dot{x}$ and from limits on the Shapiro delay. Any point outside the shaded regions is allowed by the timing data. The "median likelihood" inclination angle, indicated by a dashed vertical line, is based on an *a priori* uniform distribution in the direction of the orbital angular momentum vector. The horizontal dashed lines indicate the companion mass values expected from the $P_b - m_2$ relation for population I and II secondaries. The solid curves indicate contours of constant neutron star mass, m_1, calculated using the observed mass function for a given value of i and m_2.

the secondary,

$$(a,b,c) = \begin{cases} 4.50 & 1.2\times 10^5 & 0.120 & \text{Pop. I} \\ 4.75 & 1.1\times 10^5 & 0.115 & \text{Pop. I+II} \\ 5.00 & 1.0\times 10^5 & 0.110 & \text{Pop. II.} \end{cases} \qquad (7)$$

For the orbital period of PSR J2019+2425, $P_b = 76.512\,\mathrm{d}$, this yields masses ranging from $m_2 = 0.31\,\mathrm{M}_\odot$ for a population I donor to $m_2 = 0.35\,\mathrm{M}_\odot$ for a population II donor. These values are indicated in figure 3. In a similar analysis, Rappaport *et al.* (1995) found $0.26 < m_2 < 0.35$.

The pulsar is likely very old. Its characteristic age, calculated after correcting the observed period derivative for bias due to the translational Doppler effect, is 27 Gyr (see the discussion in Nice & Taylor 1995). Optical observations of the white dwarf secondary (Lundgren, Foster, & Camilo 1996) give a cooling age of 7.6 to 13.9 Gyr, assuming it is a helium core (Hansen & Phinney 1998). Thus the population II value of $m_2 = 0.35\,\mathrm{M}_\odot$ is likely to be appropriate for this system.

The observed mass function of the pulsar is

$$f_1 \equiv \frac{(m_2 \sin i)^3}{(m_1+m_2)^2} = \frac{4\pi^2 c^3}{G}\frac{x^3}{P_b^2} = 0.010685\,\mathrm{M}_\odot. \qquad (8)$$

For $m_2 = 0.35\,\mathrm{M}_\odot$ and $i < 72°$, this constrains the mass of the pulsar to be

$$m_1 < 1.51\,\mathrm{M}_\odot \qquad (9)$$

(see figure 3). This limit is conservative, in that it holds not just for a population II companion but for any secondary mass $m_2 < 0.35\,\mathrm{M}_\odot$, i.e., the full range of masses considered by Rappaport *et al* (1995) and Tauris & Savonije (1999). For the particular case of $m_2 = 0.35\,\mathrm{M}_\odot$, at the median likelihood value of $i = 63°$, the pulsar mass is $m_1 = 1.33\,\mathrm{M}_\odot$.

5. POLARIMETRY

Since the angular momentum of the spun-up pulsar is almost entirely due to mass transferred from the orbital companion, the angular momentum vector of the pulsar must be aligned with that of the binary system. Measurement of the geometry of the pulsar could, therefore, give the inclination of the orbit. The standard picture of pulsar radio emission along dipole magnetic field lines, the "rotating vector model" (RVM), yields a well known expression for the position angle of linearly polarized radiation, ψ, as a function of pulse phase, ϕ:

$$\psi - \psi_0 = \frac{\sin\alpha \sin(\phi-\phi_0)}{\sin\zeta\cos\alpha - \cos\zeta\sin\alpha\cos(\phi-\phi_0)}, \qquad (10)$$

where α is the angle between the rotation and magnetic axes of the pulsar, ζ is the angle between the rotation axis and the line of sight, and ϕ_0 and ψ_0 are the pulse phase and position angle at the point with the steepest change in position angle. We expect $\zeta = i$ or $\zeta = 180° - i$ for pulsar rotation aligned with the orbital angular momentum vector.

As discussed in §2, our Mark IV data includes full polarization information. Figure 4 shows a polarization profile of PSR J2019+2425 created by summing all strong Mark IV integrations. The pulsar has emission over a substantial fraction of the period and is highly linearly polarized. (An exception is that the weak component at $\phi = 60°$ is unpolarized.) Unfortunately, there is only modest variation in the position angle. This is indicative of alignment between the rotation and magnetic axes of the pulsar (small α), and in practice makes it difficult to discern ζ. We performed a grid search in ζ and α, finding the best RVM fit for each combination of these angles. The best overall fit had $\alpha = 4°$ and $\zeta = 12°$ with a $\chi^2 = 326$ for 268 degrees of freedom; this fit is plotted in figure 4. This value of ζ, 12°, is surprisingly small, and would imply a very small neutron star mass (figure 3). Though the formal significance of this fit is reasonably good, RVM fits with values of ζ ranging from 0° to 90° can be found with only a modest increase in χ^2, as shown in figure 5. The best RVM fit with $\zeta = 90°$ is also shown in figure 4; qualitatively, it does not appear very different from the overall best-fit RVM model. It should also be noted that millisecond pulsars often show deviations from the rotating vector model (e.g., Xilouris *et al.*, 1998; Stairs, Thorsett & Camilo, 1999). Because of this, we conclude that the data cannot be used to place tight limits on ζ, although within the context of the RVM we can say with confidence that $\alpha \lesssim 30°$.

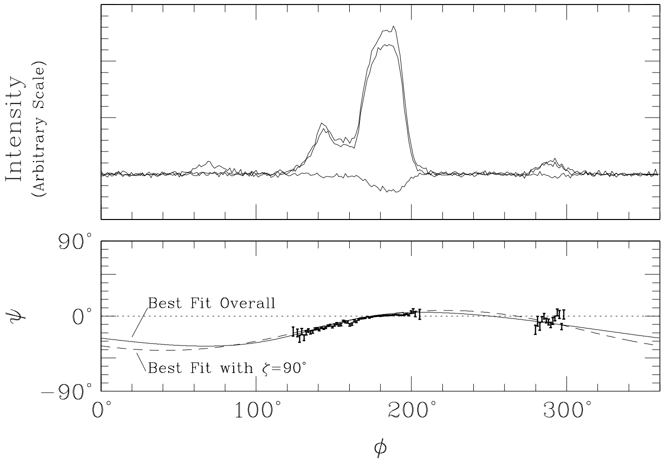

FIG. 4.— Pulse profile of PSR J2019+2425 at 430 MHz. The upper plot shows total intensity (upper trace), linearly polarized intensity (middle trace), and circularly polarized intensity (lower trace) as a function of pulse phase, ϕ. The lower plot shows the position angle of linear polarization, ψ. (Position angle is defined as increasing counterclockwise on the sky, with an arbitrary zero point.) The solid curve in the lower plot shows the overall best fit of the rotating vector model. The dashed curve shows the best RVM fit when restricted to $\zeta = 90°$. The RVM fits were performed on a 1024-bin profile, but a 256-bin profile is shown here for clarity.

6. CONCLUSION

Using two different methods, our timing observations of PSR J2019+2425 constrain the orbital inclination to be $i \lesssim 72°$. Combined with a model for evolution of the system, this limits the neutron star mass to $m_1 < 1.51\,\mathrm{M}_\odot$, with the median likelihood $m_1 = 1.33\,\mathrm{M}_\odot$ for a population II secondary. For a population I secondary the mass values would be lower.

The use of $\dot{x}$ to place an upper limit on m_1 based on a measurement of $\dot{x}$ has been used for one other pulsar. PSR J0437−4715 has $\dot{x} = 8 \times 10^{-12}$, $x = 3.367\,\mathrm{lt\text{-}s}$, $\mu = 141\,\mathrm{mas/yr}$, which gives a limit $i < 43°$ (Sandhu *et al.* 1997). When combined with the $P_b - m_2$ relation of Rappaport *et al.*, this gives $m_1 < 1.51\,\mathrm{M}_\odot$ (Thorsett & Chakrabarty 1999), coincidentally the same value as we find for PSR J2019+2425.

Our finding adds to the growing body of evidence that neutron stars in neutron-star–white dwarf orbits are not much more massive than those in neutron star–neutron star binaries. (See Thorsett & Chakrabarty 1999 for a comprehensive review of pulsar mass measurements). It is somewhat surprising that the neutron stars in these systems are not more massive, as the secondaries in these systems must lose several tenths of a solar mass as they evolve towards white dwarfs. Much of this mass could, in principle, be accreted onto the neutron stars during the low-mass X-ray binary (LMXB) phase. To keep the neutron star mass low, most of the transferred mass must leave the system, perhaps being ejected from the vicinity of the neutron star via the “propeller effect” (Illarionov & Sunyaev 1975). Taam, King & Ritter (2000) suggest that wide ($P_\mathrm{b} \gtrsim 2$ days) LMXBs are likely to be transient, with accretion occurring in short, super-Eddington outbursts that expel most of the transferred mass in a wind. Low neutron star masses such as that of PSR J2019+2425 lend strong support to this scenario.

The Arecibo Observatory is part of the National Astronomy and Ionosphere Center, which is operated by Cornell University under a cooperative agreement with the National Science Foundation. Pulsar research at Princeton University is supported by National Science Foundation grant AST96-18357. IHS received support from an NSERC postdoctoral fellowship. We thank F. Camilo, T. Tauris, and S. Thorsett for useful comments on the manuscript; A. Vázquez, F. Camilo, A. Lommen, and K. Xilouris, among others, for help with data collection; and J. Taylor for support throughout this project.

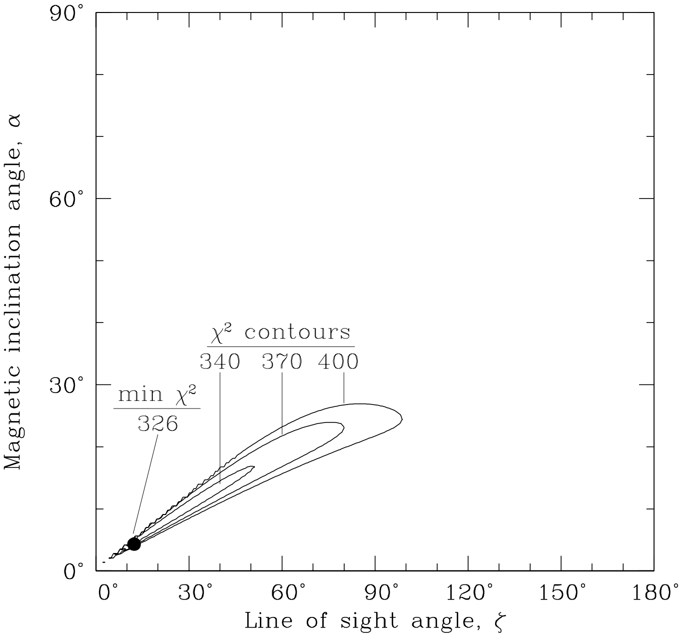

Fig. 5.— Results of fits of the rotating vector model to the linearly polarized pulse profile. Best-fitting values of the angle between the rotation and magnetic axes, α, and the angle between the rotation axis and the line of sight, ζ, are shown. Representative χ^2 values are given from fits with 268 degrees of freedom.

REFERENCES

Hansen, B. M. S. & Phinney, E. S. 1998, MNRAS, 294, 569
Illarionov, A. F. & Sunyaev, R. A. 1975, A&A, 39, 185
Kopeikin, S. M. 1996, ApJ, 467, L93
Lundgren, S. C., Foster, R. S., & Camilo, F. 1996, in Pulsars: Problems and Progress, IAU Colloquium 160, ed. S. Johnston, M. A. Walker, & M. Bailes, (San Francisco: Astronomical Society of the Pacific), 497
Nice, D. J. & Taylor, J. H. 1995, ApJ, 441, 429
Nice, D. J., Taylor, J. H., & Fruchter, A. S. 1993, ApJ, 402, L49
Peters, P. C. 1964, Phys. Rev., 136, 1224
Rappaport, S., Podsiadlowski, P., Joss, P. C., DiStefano, R., & Han, Z. 1995, MNRAS, 273, 731
Sandhu, J. S., Bailes, M., Manchester, R. N., Navarro, J., Kulkarni, S. R., & Anderson, S. B. 1997, ApJ, 478, L95
Stairs, I. H., Splaver, E. M., Thorsett, S. E., Nice, D. J., & Taylor, J. H. 2000, MNRAS, 314, 459
Stairs, I. H., Thorsett, S. E., & Camilo, F. 1999, ApJS, 123, 627
Stinebring, D. R., Kaspi, V. M., Nice, D. J., Ryba, M. F., Taylor, J. H., Thorsett, S. E., & Hankins, T. H. 1992, Rev. Sci. Instrum., 63, 3551
Taam, R. E., King, A. R., & Ritter, H. 2000, ApJ. in press, astro-ph/0007055
Tauris, T. M. & Savonije, G. J. 1999, A&A, 350, 928
Thorsett, S. E. & Chakrabarty, D. 1999, ApJ, 512, 288
Xilouris, K. M., Kramer, M., Jessner, A., von Hoensbroech, A., Lorimer, D., Wielebinski, R., Wolszczan, A., & Camilo, F. 1998, ApJ, 501, 286